Macromolecules
ARTICLE

Macromolecules **2009**, *42*, 8925–8932 **8925**
DOI: 10.1021/ma901647b

Microphase Separation in Sulfonated Block Copolymers Studied by Monte Carlo Simulations

P. Knychała,[†] M. Banaszak,*[,†] M. J. Park,[‡] and N. P. Balsara[§]

[†]*Faculty of Physics, A. Mickiewicz University ul. Umultowska 85, 61-614 Poznan, Poland,* [‡]*Department of Chemistry and Division of Advanced Materials Science, Pohang University of Science and Technology (POSTECH), Pohang 790-784, Korea, and* [§]*Department of Chemical Engineering, University of California, Materials Sciences Division and Environmental Energy Technologies Division, Lawrence Berkeley National Laboratory, University of California, Berkeley, California 94720*

Received July 25, 2009; Revised Manuscript Received September 11, 2009

ABSTRACT: The underpinnings of microphase separation in symmetric poly(styrenesulfonate-*block*-methylbutylene) (PSS−PMB) copolymer melts were examined by Monte Carlo lattice simulations. The main challenge is understanding the effect of ion pairs in the PSS block on thermodynamics. We assume that experimentally determined Flory−Huggins interaction parameters are adequate for describing intermonomer interactions. Our model does not account for either electrostatic or dipolar interactions. This enables comparisons between simulated and experimentally observed microphases reported by Park and Balsara [*Macromolecules* **2008**, *41*, 3678] without resorting to any adjustable parameters. The PSS block in both experiments and theory is partially sulfonated. We quantified the effect of sequence distribution on phase behavior by using alternating and blocky PSS chains in the simulations. Depending on temperature and sequence distribution, simulations show perforated lamellae, gyroid, and hexagonally packed cylinders in addition to the lamellar phase found in simple symmetric block copolymers that do not contain ions. This is driven by extremely repulsive interactions between styrenesulfonate monomers and the uncharged species in the melts. The symmetry of the microphases and the locations of the order−disorder and order−order phase transitions are in qualitative agreement with experimental observations.

I. Introduction

There is considerable interest in composite membranes that transport ions in energy-related applications such as batteries and fuel cells.[1−3] These membranes often comprise ion-conducting channels in an insulating matrix. An example of such a system is Nafion, which is a linear random copolymer of sulfonated and nonsulfonated fluoroalkyl groups. Thermodynamic incompatibility of the ionic and nonionic species leads to microphase separation, resulting in the spontaneous assembly of conducting and nonconducting domains. The purpose of this article is to describe molecular modeling efforts to understand the underpinnings of self-assembly of ion-containing copolymers. In this initial study, we restrict our attention to neat copolymers in the absence of additives such as water and salt.

Block copolymers provide a logical starting point for understanding the self-assembly of ion-containing copolymers. Extensive experimental and theoretical studies on uncharged block copolymers serve as the basis for developing such an understanding.[4−12] In the case of diblock copolymers, for example, knowledge of the Flory−Huggins interaction parameter, χ, which quantifies the magnitude of dispersive interactions between monomers, and the statistical segment lengths of the two blocks enable theoretical prediction of geometry, size, and stability windows of the microphase-separated morphologies. The agreement between predictions of self-consistent field theory, simulations, and experiment is excellent. Recent advances in field theoretic simulations[13] demonstrate, however, that inclusion of field fluctuations (beyond the self-consistent mean-field approximation) is crucial for quantification of microphase separation in these systems. Particle simulations of block copolymers pose a considerable challenge because of the finite size effects.[14] In this work, we use a lattice model because lattice simulations are more efficient (compared with continuum simulations) while capturing the essential physics of uncharged block copolymer assembly, as, for example, in ref 15.

A recent experimental study reported on the phase behavior of polystyrenesulfonate-*block*-polymethylbutylene (PSS−PMB copolymers).[16] A variety of morphologies, lamellae, gyroid, hexagonally perforated lamellae, and hexagonally packed cylinders, were obtained in nearly symmetric PSS−PMBs with PSS volume fractions between 0.45 and 0.5. In this range of compositions, only lamellar phases are seen in uncharged block copolymers. It is therefore clear that self-assembly of sulfonated block copolymers is radically different from that of uncharged block copolymers. The ions in PSS−PMB copolymers are embedded in a low dielectric medium (polystyrene and perhaps polymethylbutylene) wherein the anions and cations are expected to be bound in the form of ion pairs. Classical theories suggest that such pairs can often be approximated as neutral dipolar molecules.[17] In addition, it has been shown that electrostatic interactions in dense copolymer melts with ion pairs are screened out if the characteristic length of electrostatic screening is smaller than the effective segment size.[18] It may thus be possible to use simple models based on χ parameters to describe the thermodynamic properties of PSS−PMB systems.

Whereas the experimental system is a randomly sulfonated copolymer (with chains differing in distribution of sulfonated segments) with finite polydispersity, in simulation, we use three models with identical chains. In contrast with the experimental random copolymer system, all chains in a particular simulation have the same sequence distribution. We probe if this simple

*Corresponding author. E-mail: mbanasz@amu.edu.pl.

Published on Web 09/30/2009

model is sufficient for a qualitative insight into the phase behavior of the complex experimental system. The value of the χ parameter between sulfonated polystyrene and polystyrene, χ_{S-SS}, reported in ref 16, is 6.54, which is at the low end of the range of χ parameters reported in the literature for this system; the literature values range from 5 to 25.[19,20]

Our objective is to answer three fundamental questions: (1) Are χ values as high as 6 physically meaningful, or are they a reflection of the inability of theories originally developed for weak dispersive interactions to describe interactions with ion pairs? It is clear, for example, that predicting the phase behavior of critical binary blends of PSS and PS is impossible because setting $\chi N = 2$ at the critical point, where N is the number of monomers per chain in both homopolymers, leads to a fractional value for N. Is the large disparity in the measured χ parameters reported in the literature for this system also an indication of the inapplicability of the simple theories of polymer−polymer interactions? (2) Can we use these large χ parameters to explain the presence of nonlamellar phases in symmetric PSS−PMB copolymers? If this is not the case, then it may be necessary to construct more complicated models that explicitly account for the presence of charged species in our monomers. (3) What is the effect of sequence distribution on the observed phase behavior? The sulfonated PSS blocks are synthesized by randomly sulfonating PS blocks. Whereas it is generally assumed that the sulfonation is random, there is a radical change in the solubility of PS upon sulfonation from highly hydrophobic to highly hydrophilic. This may lead to unexpected sequence distributions because of the formation of micelle-like structures in solution, the dependence of the reactivity of unreacted styrene monomers on the local concentration of charged styrenesulfonate monomers, and so on.

In this article, we use a lattice Monte Carlo (MC) method with the cooperative motion algorithm (CMA)[21,22] developed by Pakula and coworkers[23] to model the phase behavior of PSS−PMB block copolymers. Interactions between the PSS and PMB monomers are accounted for by introducing χ parameters. The CMA model is built of a lattice liquid rather than a lattice gas and thus does not require vacancies to undergo rearrangements. This makes the approach ideally suited for dense polymeric systems. The χ parameters used in the simulations were taken from ref 16. The simulations and experiments can thus be compared without resorting to adjustable parameters.

II. Model and Method

The simulations are performed using CMA for a face-centered cubic (FCC) lattice with the coordination number $z = 12$ and the bond length $\sqrt{2}a$, where a is the FCC lattice constant, used also as a length unit. Chain bonds are not allowed to be broken or stretched, and the usual periodic boundary conditions are imposed. The lattice box size is chosen to fit the chain, and the lattice sites are completely filled with chain segments; there are no vacancies. Because all lattice sites are occupied, a chain segment can move if other segments move simultaneously. An attempt to move a single segment defines a single MC step.

We model the PSS−PMB copolymer by a linear lattice chain consisting of 34 segments ($N = 34$), with segments of type A, S, and B corresponding to PS, PSS, and PMB, respectively. The model copolymer chain is symmetric, which means that we have 17 segments of type B and 17 segments of the other two types (A or S). To have a similar level of sulfonation as that reported in ref 16, we choose 7 segments of type S, and 10 segments of type A. The fraction of sulfonated segments in the A/S block, p, is 0.415. The chain length that we use, $N = 34$, is a realistic compromise between our desire to simulate long chains and the computing powers at our disposal. Because the sequence of sulfonated segments in the PSS block is not known from experiment, we assume three different sequence distributions for the S-segments, shown in Figure 1. The first distribution sequence is an alternating (ALT) copolymer with one S segment, followed by one A segment, except near the block junction, as shown in Figure 1a. The second sequence distribution, has alternating three A and two S blocks, referred to as two-block (2B), as shown in Figure 1b. The third sequence distribution has an S block in the middle, surrounded by two A blocks, referred to as one-block (1B), as shown in Figure 1c. The blockiness of the model PSS block increases in the order ATL, 2B, and 1B. It is evident that we are not attempting to understand the role of quenched disorder on the self-assembly of PSS−PMB copolymers, as has been done in refs 24−27.

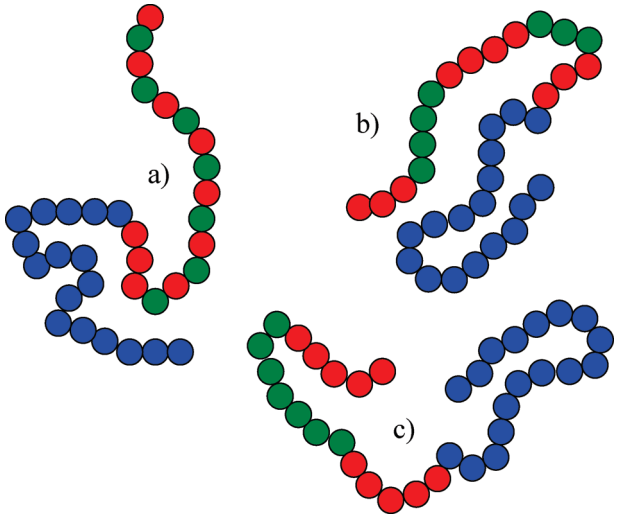

Figure 1. Three types of sequence distributions used for realistic ϵ values: (a) ALT, (b) 2B, and (c) 1B. Segments of type A are indicated in red, segments of type S are indicated in green, and segments of type B are indicated in blue.

The intermonomer interactions are limited to the nearest neighbors ($z = 12$), and the Flory interaction parameter between monomers, χ_{ij}, is related to the interaction energies, ϵ_{ij}, by the following equation

$$\chi_{ij} = \frac{(z-2)(\epsilon_{ij} - (\epsilon_{ii} + \epsilon_{jj})/2)}{kT} \quad (1)$$

Whereas other values of z can be used, as, for example, in refs 28 and 29, limiting the interactions to the nearest neighbors is the simplest approach. We further simplify the system by assuming that $\epsilon_{AA} = \epsilon_{BB} = \epsilon_{SS} = 0$, and thus

$$\chi_{ij} = \frac{(z-2)\epsilon_{ij}}{kT} \quad (2)$$

This enables us to estimate ϵ_{ij} from experimental measurements of χ_{ij}. Using the data in ref 16, we thus obtain

$$\epsilon_{AB} = 0.042\epsilon \quad (3)$$

$$\epsilon_{BS} = 0.792\epsilon \quad (4)$$

$$\epsilon_{AS} = \epsilon \quad (5)$$

We refer to this set of parameters as "realistic" parameters. Note, however, that ϵ_{AS} and ϵ_{BS} are significantly greater than ϵ_{AB}. We can thus introduce a "simplistic" model where

$$\epsilon_{AB} = 0 \quad (6)$$

$$\epsilon_{AS} = \epsilon_{BS} = \epsilon \quad (7)$$

The simplistic model (Figure 2) makes 1B and 2B systems equivalent to triblock and pentablock copolymers, respectively.

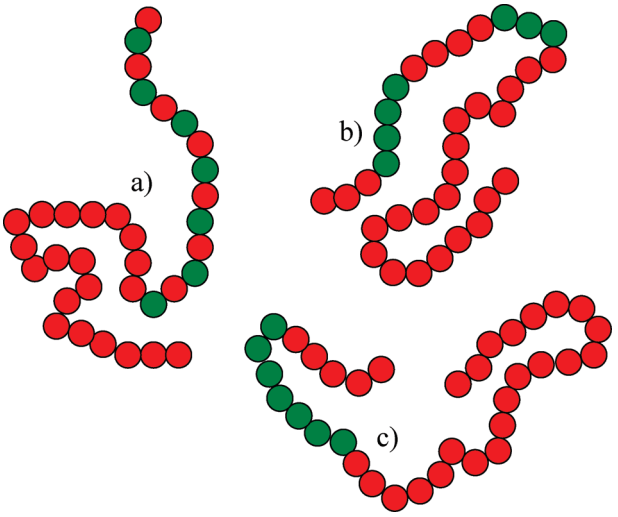

Figure 2. Three types of sequence distributions used for simplified ϵ values: (a) ALT, (b) 2B, and (c) 1B. Segments of type A and B are indicated in red, and segments of type S are indicated in green.

This enables the definitions of reduced energies and temperatures.

$$\frac{E^*}{n_a} = \frac{(E/\epsilon)}{n_a} \tag{8}$$

$$T^* = \frac{kT}{\epsilon} \tag{9}$$

where n_a is the number of lattice sites, E is the total energy, and E^* is the reduced energy in units of ϵ. Similarly, T^* is the reduced temperature in units of k_BT. Because the simulations are done at constant volume, heat capacity, C_v, is then given by

$$C_v = \frac{\langle (E^* - \langle E^* \rangle)^2 \rangle}{n_c T^{*2}} \tag{10}$$

where $\langle \cdots \rangle$ denotes thermal averaging, and n_c is the number of chains. It should be noted that positive ϵ values do not mean that we neglect attractive forces. In fact, as shown, for example, by de Gennes[30] for an incompressible melt, individual ϵ values can be negative, but the effective ϵ (and also χ) values are positive. For simplicity, we assume that $\epsilon_{AA} = \epsilon_{BB} = \epsilon_{SS} = 0$, and the effective ϵ values (and χ as expressed in eq 1) between different segments are positive (or sometimes zero) without the loss of generality.

We use a $34 \times 34 \times 34$ FCC box (with $n_a = 34^3/2 = 19\,652$ sites) to fit a fully extended 17−17 copolymer chain. The FCC lattice is generated from a simple cubic $34 \times 34 \times 34$ lattice by removing every second site (to satisfy the condition that the sum of integer coordinates, $x + y + z$, is an odd integer). For the copolymer melt, the whole FCC lattice is filled with copolymer chains, which means that there are $n_a/N = 578$ chains. The absence of voids precludes the possibility of studying the interaction between density and concentration fluctuations, which may be important in these systems. We investigate the size effects by performing simulations in boxes of various sizes. In particular, we carry out selected studies for the $68 \times 68 \times 68$ box, with the number of copolymer chains being 8 times greater than that for the initial box ($34 \times 34 \times 34$). We perform a series of simulations for at least 30 (30, 73, and 43 for ALT, 2B, and 1B, respectively) different temperatures, T, for the smallest box, and for the larger box, we simulate at selected temperatures of interest.

First, we equilibrate the system in the athermal limit, that is, where $\epsilon/(kT)$ is zero. When the system reaches its thermal equilibrium, the polymer chains assume statistical conformations and random orientations and become uniformly distributed within the simulation box. From the equilibrated melt state, the system is quenched to any required temperature. This procedure is fully described in refs 31 and 32. We perform at least 5×10^6 MC steps and repeat the simulation at least three times starting with different initial states. For a given state point, all runs yield the same type of nanostructure, and the results are averaged over all such runs. We also verify the quality of thermal equilibration by heating the system up and then cooling it down again. Usually, we also assume that the first half of the run is needed to equilibrate the system and the second half is used to collect the data.

Table 1. Peak Positions of the Structure Factor for Various Nanostructures[a]

nanostructure	ratio k/k^*						
L	1	2	3	4	5	6	...
HPC ($P6mm$)	1	$\sqrt{3}$	$\sqrt{4}$	$\sqrt{7}$	$\sqrt{9}$	$\sqrt{12}$	...
DD ($Pn\bar{3}m$)	1	$(3/2)^{1/2}$	$\sqrt{2}$	$\sqrt{3}$	$\sqrt{4}$	$(9/2)^{1/2}$	...
G ($Ia\bar{3}d$)	1	$(4/3)^{1/2}$	$(7/3)^{1/2}$	$(8/3)^{1/2}$	$(10/3)^{1/2}$	$(11/3)^{1/2}$	...

[a] L stands for lamellae, HPC stands for hexagonally packed cylinders, DD stands for double diamond, and G stands for gyroid, where k^* is the magnitude of the wavevector at the primary diffraction peak.

The structure factor, $S(k)$, is calculated by averaging over statistically independent configurations using the following equation

$$S(\vec{k}) = \frac{1}{n_\alpha} \left\langle \left(\sum_{m=1}^{n_\alpha} \cos(\vec{k} \cdot \vec{r}_m) \right)^2 + \left(\sum_{m=1}^{n_\alpha} \sin(\vec{k} \cdot \vec{r}_m) \right)^2 \right\rangle_{\text{thermal average}} \tag{11}$$

where n_α denotes the number of segments of type α and $\vec{r}_m$ denotes the position of the mth segment of type α; for sulfonated segments, $\alpha = S$. The magnitude of the wavevector, k, varies from $k_{min} = 2\pi/L$ to $k_{max} = 2\pi/b$, where L is the size of the cubic simulation box, and b is the distance between nearest segments, equal to $\sqrt{2}$ ($a = 1$), on the FCC lattice. Moreover, $\vec{k}$ vectors are commensurate with the simulation box size, and this constraint limits their number and allowed lengths. Because the system may not be isotropic, $S(k)$ is calculated by averaging over all $S(\vec{k})$ such that $|\vec{k}|$ is equal to k. We use peaks in $S(k)$ to identify the self-assembled nanostructures using well-known diffraction results that are summarized in Table 1. We calculate ensemble-averaged energy per lattice site, E^*/n_a, heat capacity, C_v, copolymer chain end-to-end distance, R^2, and structure factor, $S(k)$, for each temperature, T^*, in the range $T^* = 1$ to 10.

III. Results and Discussion

Typical results for the energy per lattice site, E^*/n_a, heat capacity, C_v, and mean squared end-to-end distance of the copolymer chain, R^2, as a function of T^* are shown in Figure 3, where data obtained for 2B using both the realistic and simplified ϵ values are shown. Whereas there are some differences seen in the two data sets, the general trends obtained from the two sets of ϵ values are similar. The decrease in E^* and the peak in C_v seen in the realistic model indicate the presence of a phase transition. There are also sharp changes in R^2 at certain values of T^*. Qualitatively similar trends were obtained in ALT and 1B.

To obtain further insight into the phase behavior of the melts, we show snapshots of representative configurations at selected T^* values for the realistic model in Figure 4. In cases where the structure is not trivial to discern, we show only the S mononers in green (e.g., Figure 4c,e,f). ALT exhibits a lamellar phase at low temperatures, as shown in Figure 4a, and disorder at high temperatures (not shown for brevity). 2B exhibits lamellar and gyroid phases at $T^* = 1.67$ and 1.92, respectively, as shown Figure 4b,c. Figure 1B exhibits lamellae, gyroid, and hexagonally

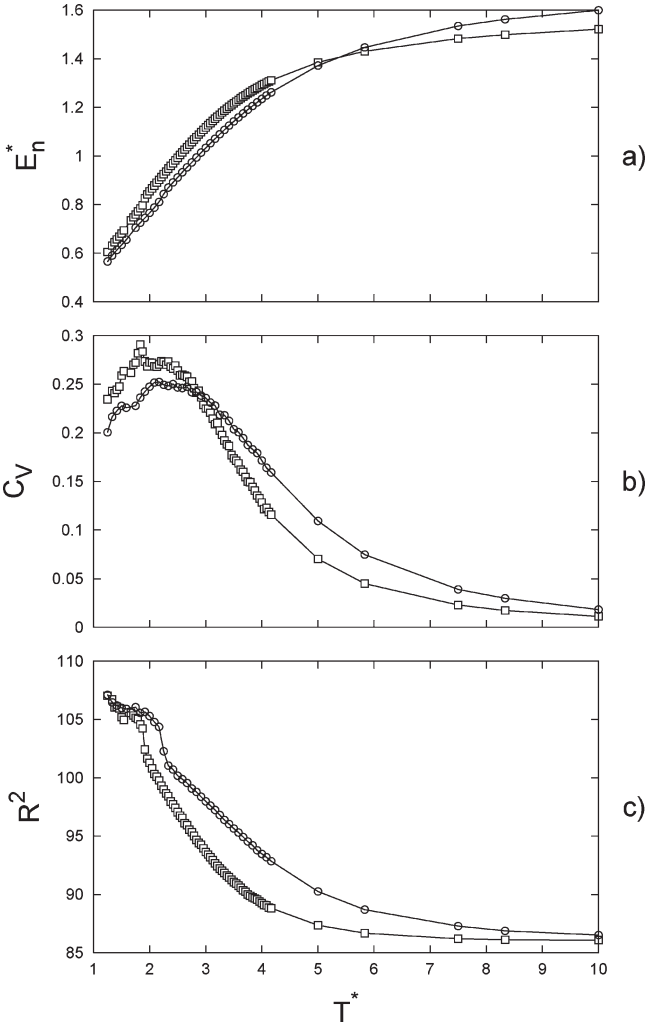

Figure 3. Simulation results for 2B sequence distribution, simplified ϵ values (circle) and realistic ϵ values (square): (a) energy per lattice site, E_n^*, (b) heat capacity, C_v, and (c) squared end-to-end distance, R^2.

packed cylinders at $T^* = 1.5$, 2.25, and 2.58, respectively. The S/A block forms the cylinder phase at $T^* = 2.58$, with the S block in the middle of the cylinders (Figure 4f), the A block covering S-cylinders (Figure 4g), and the B block forming the matrix phase. This is not surprising because whereas the volume fraction of the S/A block in the simulations is 0.5, the self-assembly is driven by the incompatibility of the S block with both A and B segments, and the volume fraction of the S block is 0.21. The experimental data in ref 16 obtained by both scattering and microscopy did not distinguish between PSS and PS monomers. The simulations provide insight into the possible arrangements of these components. In Figure 4h, we show data obtained at $T^* = 2.92$. Whereas the box clearly contains an ordered continuous phase, we were unable to determine the symmetry of the phase from the simulation data. Possible reasons for this are discussed below. We use the term "continuous" morphology to refer to this phase.

Snapshots of representative configurations at selected T^* values for the simplistic model are shown in Figure 5. The lamellar structures in the ALT sample at $T^* = 1.17$ and 2.0, shown in Figure 5a,b, exhibit important differences. At $T^* = 2.0$, we see evidence of the B monomers perforating the S/A lamellae, as can be seen in the top face of Figure 5b. Despite the extensive analysis of both snapshots and $S(k)$ data, we were unable to determine if the perforations were ordered or disordered. We were also unable to distinguish clearly between perforated

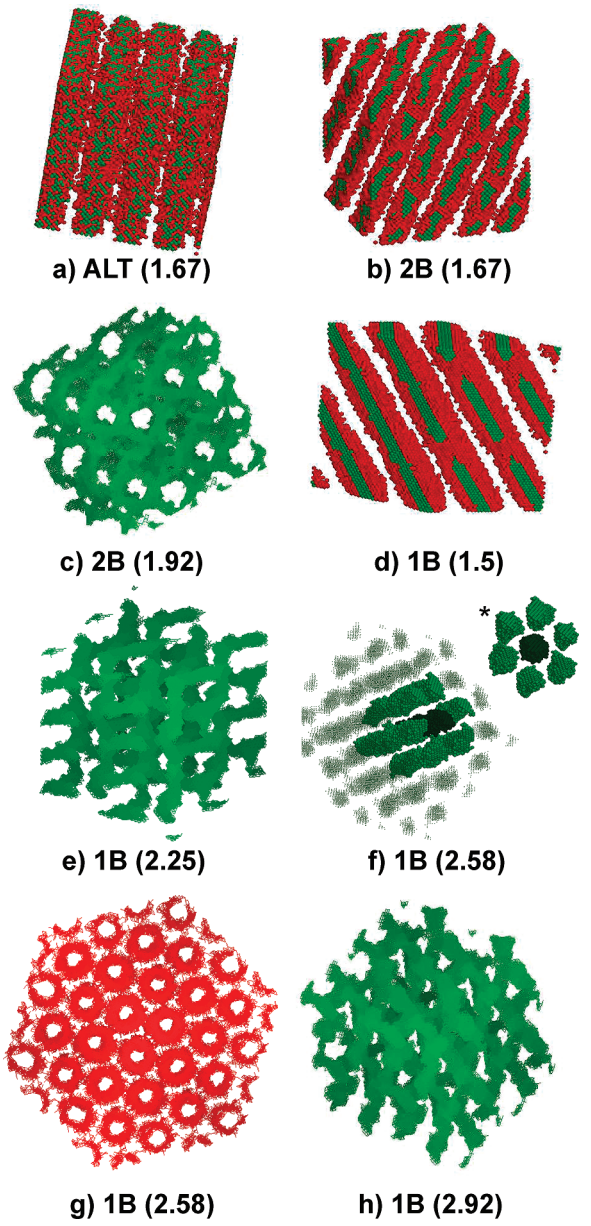

Figure 4. Snapshots of representative configurations for realistic ϵ values: (a) ALT: lamellar phase at $T^* = 1.67$, (b) 2B: lamellar phase at $T^* = 1.67$, (c) 2B: gyroid phase at $T^* = 1.92$, (d) 1B: lamellar phase at $T^* = 1.5$, (e) 1B: gyroid phase at $T^* = 2.25$, (f) 1B: HPC nanostructure at $T^* = 2.58$ (seven S-cylinders are shown in a hexagonal arrangement; the central cylinder is shown in a darker shade of green), (g) 1B: HPC nanostructure at $T^* = 2.58$ (A-layers surrounding S-cylinders in hexagonal arrangement), (h) 1B: continuous nanostructure at $T^* = 2.92$. Colors used are the same as those in Figure 1.

(PL) and nonperforated (L) lamellae. This was true in all cases. Some simulations would clearly show perforations, whereas others did not. We thus refer to the lamellar phase as the L/PL phase.

The fact that simulations of 1B and 2B systems lead to nonlamellar phases is not surprising because microphase separation is mainly driven by the repulsion between the sulfonated and nonsulfonated monomers and the volume fraction of the sulfonated segments is 21% in all of the model systems. However, it is evident that complex phases such as perforated lamellae can arise at equilibrium even in the simple case of a symmetric diblock copolymer with an alternating block. Note that in the case of simple uncharged systems, there is scant attention paid to the alternating nature of most monomers. For example, polystyrene

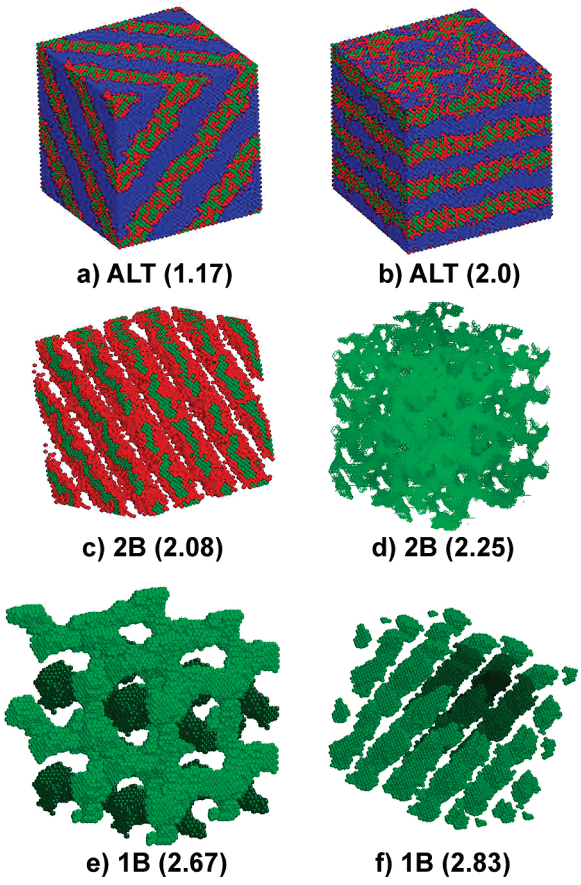

Figure 5. Snapshots of representative configurations for simplified ϵ values: (a) ALT: lamellar phase at $T^* = 1.17$, (b) ALT: lamellar phase at $T^* = 2.0$, (c) 2B: lamellar phase with perforations at $T^* = 2.08$, (d) 2B: continuous nanostructure at $T^* = 2.25$, (e) 1B: gyroid nanostructure at $T^* = 2.67$ (only sulfonated segments shown in two different shades of green), (f) 1B: HPC nanostructure at $T^* = 2.83$ (seven cylinders are shown in a hexagonal arrangement). Colors used are the same as those in Figure 2.

is an alternating copolymer with one CH_2 subunit and one C_7H_6 subunit. All thermodynamic treatments of polystyrene regard these chains as homopolymers; that is, the two alternating subunits are coarse-grained into a single monomer unit.[33] The data in Figure 5b suggest that coarse graining has to be done more carefully in the case of systems with very large χ parameters (or, perhaps when one of the monomers contains charged species). The structures obtained in 2B with the simplistic model (Figure 5c,d) are similar to those obtained with the realistic model (Figure 4b,c). The same applies to 1B; compare Figure 4e,f with Figure 5e,f.

We identified transitions between the phases described above by examining $S(k)$. We focus on the realistic model because of our desire to compare our simulations with experiments reported in ref 16. The $S(k)$ values are calculated by averaging over 10^3 statistically independent configurations using eq 11. Figure 6 shows results obtained for $S(k)$ of the S monomers of ALT using the realistic model. As seen in Figure 6a, at high temperatures, we observe a single broad peak characteristic of a disordered phase. As the temperature is decreased, we observe higher-order peaks, indicating the presence of a lamellar phase (Table 1). We take the emergence of higher-order peaks to be a signature of a transition from disorder to order. The large number of simulations undertaken (Figure 6a) enables unambiguous determination of the transition temperature. Typical $S(k)$ data obtained in the ordered and disordered states are shown in Figure 6b,c, respectively. Similar analysis of 2B data is shown in Figure 7 (S monomers). Here we show $S(k)$ data for the three structures seen in this

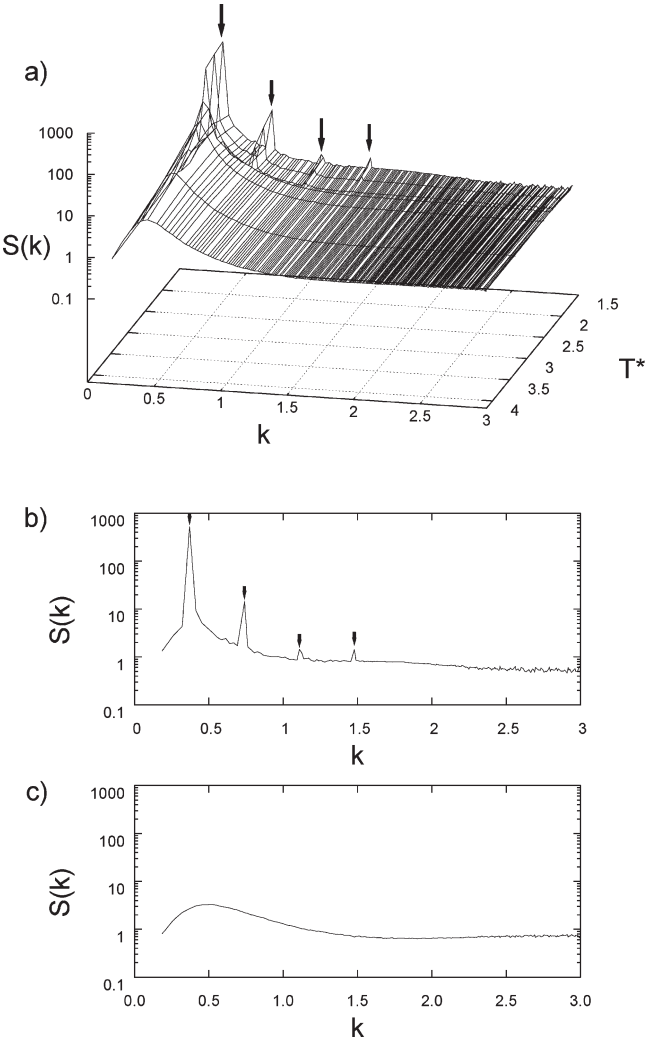

Figure 6. S-segments structure factor for ALT and realistic ϵ values: (a) as a function of T^* and k, (b) at $T^* = 1.67$ (1, 2, 3, and 4 peaks indicate L phase), and (c) at $T^* = 10.0$ (disordered phase).

polymer: a high-temperature disordered phase, a gyroid phase at intermediate temperatures, and a lamellar phase at low temperatures.

The S-segment $S(k)$ of 1B (realistic model), exhibiting the unidentifiable continuous phase at $T^* = 2.92$ (note Figure 4h), is shown in Figure 8a. In Figure 8b,c, we show S-segment $S(k)$ of 1B from using the realistic and simplistic models, respectively. The $S(k)$ from both realistic and simplistic systems shows a gyroid morphology, which is consistent with snapshots given in Figures 4e and 5e, respectively. Whereas the values of T^* are different, the qualitative similarity of the phase behavior obtained from the two models is seen in both position and reciprocal space. We examined the arrangement of B segments, or equivalently (A + S) segments, and found no additional information. From both $S(k)$ and snapshots, we observe that if S forms a certain type of nanophase, then (A + S) forms the same type of nanophase. An example of this is shown in Figure 8d, where we show the B-segment $S(k)$ for 1B using the realistic model at $T^* = 2.25$. Here we see scattering peaks of the G phase, which are very similar to those reported in Figure 8b, where the S-segment $S(k)$ is given for the same case. Clear scattering peaks of 1B corresponding to the HPC phase are not shown for brevity. Some of the expected higher-order peaks of complex morphologies, such as the G phase, are within the noise in $S(k)$, as is the case in the data in Figure 7b. Our assignment of morphology is based on a combination of snapshots in position space (e.g., Figure 4c) and $S(k)$.

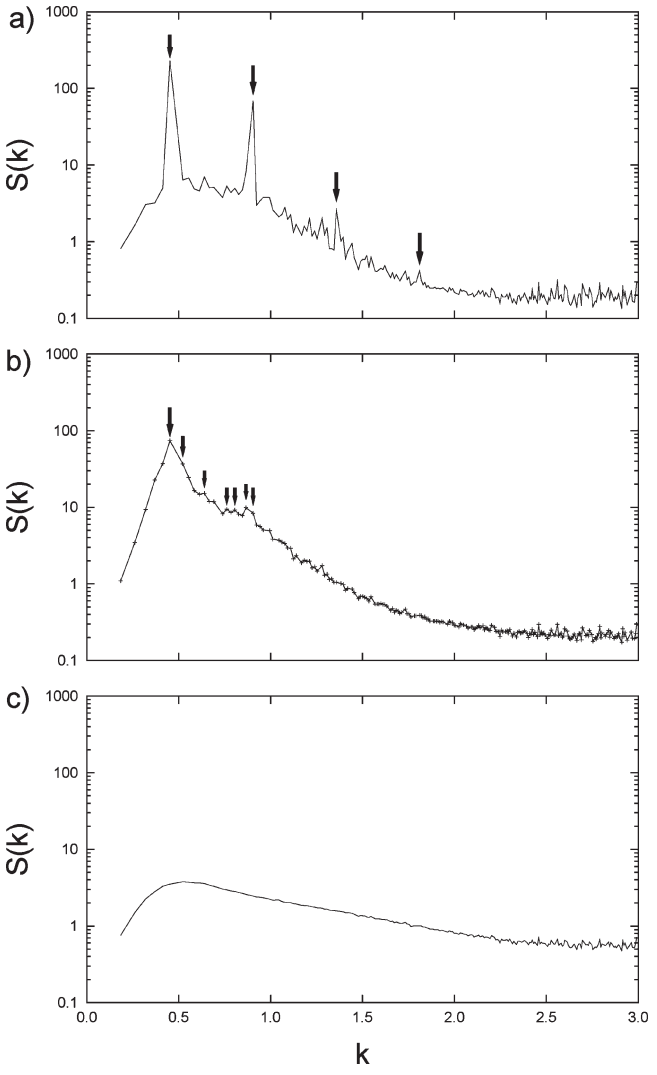

Figure 7. S-segment structure factor for 2B and realistic ϵ values at selected temperatures: (a) $T^* = 1.67$ (1, 2, 3, and 4 peaks indicate L phase), (b) $T^* = 1.92$ (1, $(4/3)^{1/2}$, $(7/3)^{1/2}$, $(8/3)^{1/2}$, $(10/3)^{1/2}$, $(11/3)^{1/2}$, and $(12/3)^{1/2}$ indicate peaks of G phase), and (c) $T^* = 10.0$ (disordered phase).

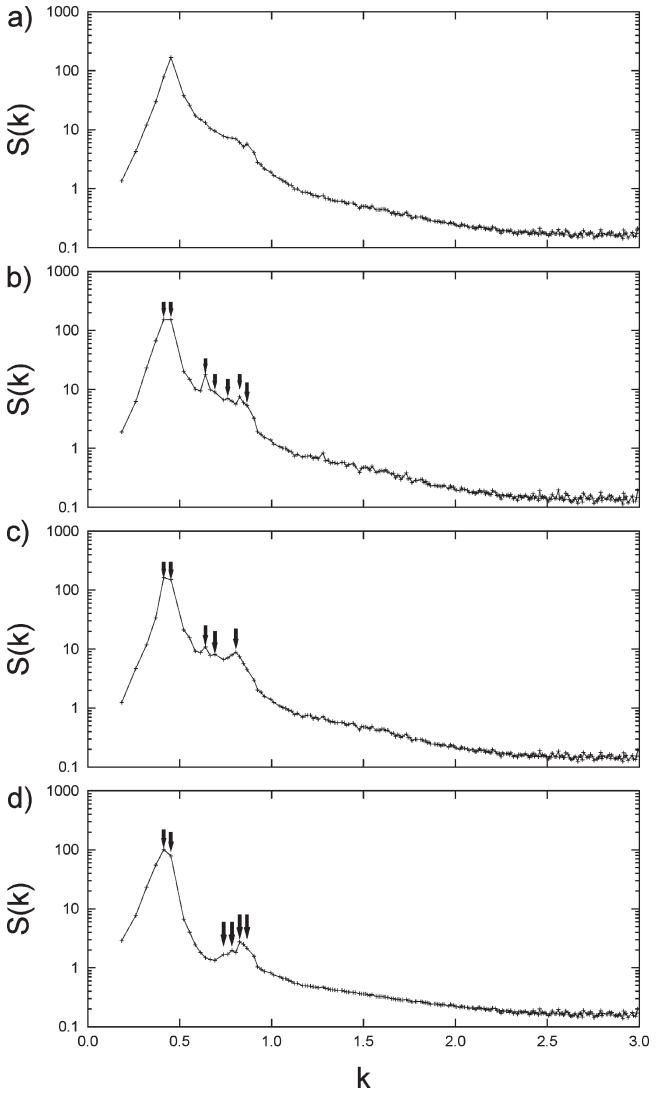

Figure 8. (a,b,c) S-segment and (d) B-segment structure factors for 1B at selected temperatures: (a) $T^* = 2.92$ − realistic ϵ values (peaks do not indicate a known phase), (b) $T^* = 2.25$ - realistic ϵ values (1, $(4/3)^{1/2}$, $(7/3)^{1/2}$, $(8/3)^{1/2}$, $(10/3)^{1/2}$, $(12/3)^{1/2}$, and $(13/3)^{1/2}$ peaks indicate G phase), (c) $T^* = 2.67$ − simplified ϵ values (1, $(4/3)^{1/2}$, $(7/3)^{1/2}$, $(8/3)^{1/2}$, and $(11/3)^{1/2}$ peaks indicate G phase), and (d) $T^* = 2.25$ − realistic ϵ values (1, $(4/3)^{1/2}$, $(10/3)^{1/2}$, $(11/3)^{1/2}$, $(12/3)^{1/2}$, and $(13/3)^{1/2}$ peaks indicate G phase).

Figure 9a shows observed phases for three different sequence distributions (ALT, 2B, and 1B) and summarizes the main results of this work. We express these results in terms of $p^2\chi N$, where $N = 34$, χ is calculated from eq 2, and $p = 0.415$ is the sulfonation fraction of the A/S block. Note that $p^2\chi$ can be thought of as an effective interaction parameter between charged (A/S) and uncharged (B) segments in the spirit of random copolymer theory (RCT).[16] ALT exhibits an ODT at $p^2\chi N = 27$ ($T^* = 2.2$). 2B exhibits two transitions, first an ODT at $p^2\chi N = 23$ ($T^* = 2.5$) to a gyroid nanophase and then the OOT to the L/PL nanophase at $p^2\chi N = 31$ ($T^* = 1.88$). 1B exhibits an ODT to the continuous phase at $p^2\chi N = 17$ ($T^* = 3.5$), followed by an OOT at $p^2\chi N = 20$ ($T^* = 2.85$) to HPC. Above $p^2\chi N = 23$ ($T^* = 2.5$), we observe a G nanophase, and at $p^2\chi N = 35$ ($T^* = 1.66$), we observe an OOT to L/PL phase.

Figure 9b shows the experimental data obtained from symmetric PSS−PMB copolymers given in ref 16. The data were obtained on samples with $N = 54$ and 99. The two panels in Figure 9b show data obtained at two sulfonation levels of 32 and 44 mol %, corresponding to $p = 0.38$ and 0.51, respectively. The qualitative features seen in both panels are similar. The sample with $N = 54$ exhibited an ODT to a gyroid phase, whereas the sample with $N = 99$ exhibited a lamellar to hexagonally perforated lamellar phase. We use the simplistic model with $\chi = p^2 \times 6.54 \times 298/T$, assuming that the value of 6.54 obtained at room temperature can be extrapolated to higher temperature using a $1/T$ relationship. The solid lines in Figure 9b represent ODTs and OOTs, whereas the dashed lines represent the limits of the experimental window. The experimental ODTs occur at $p^2\chi N = 47$ ($p = 0.38$) and 66 ($p = 0.51$), compared with the simulation ODTs that occur at 27 (ALT), 23 (2B), and 17 (1B). As indicated in Figure 9b, there were no direct experimental observations of an OOT from G to L. However, in both $p = 0.38$ and $p = 0.51$ samples, we find that increasing N from 54 to 99 results in a G-to-L transformation. We use the limits of the experimental windows to estimate the range of values of $p^2\chi N$ over which a G-to-L transition is obtained. The experimental OOT from G to L thus obtained occurs at $p^2\chi N$ between 51 and 66 ($p = 0.38$; two dashed lines in the middle of Figure 9b) and 90 and 117 ($p = 0.51$). The G-to-L/PL transition in simulations is observed at $p^2\chi N = 31$ (2B) and 35 (1B). The experimentally observed G to L OOTs that occur at 86 ($p = 0.38$) and 136 ($p = 0.51$) could not be addressed by our

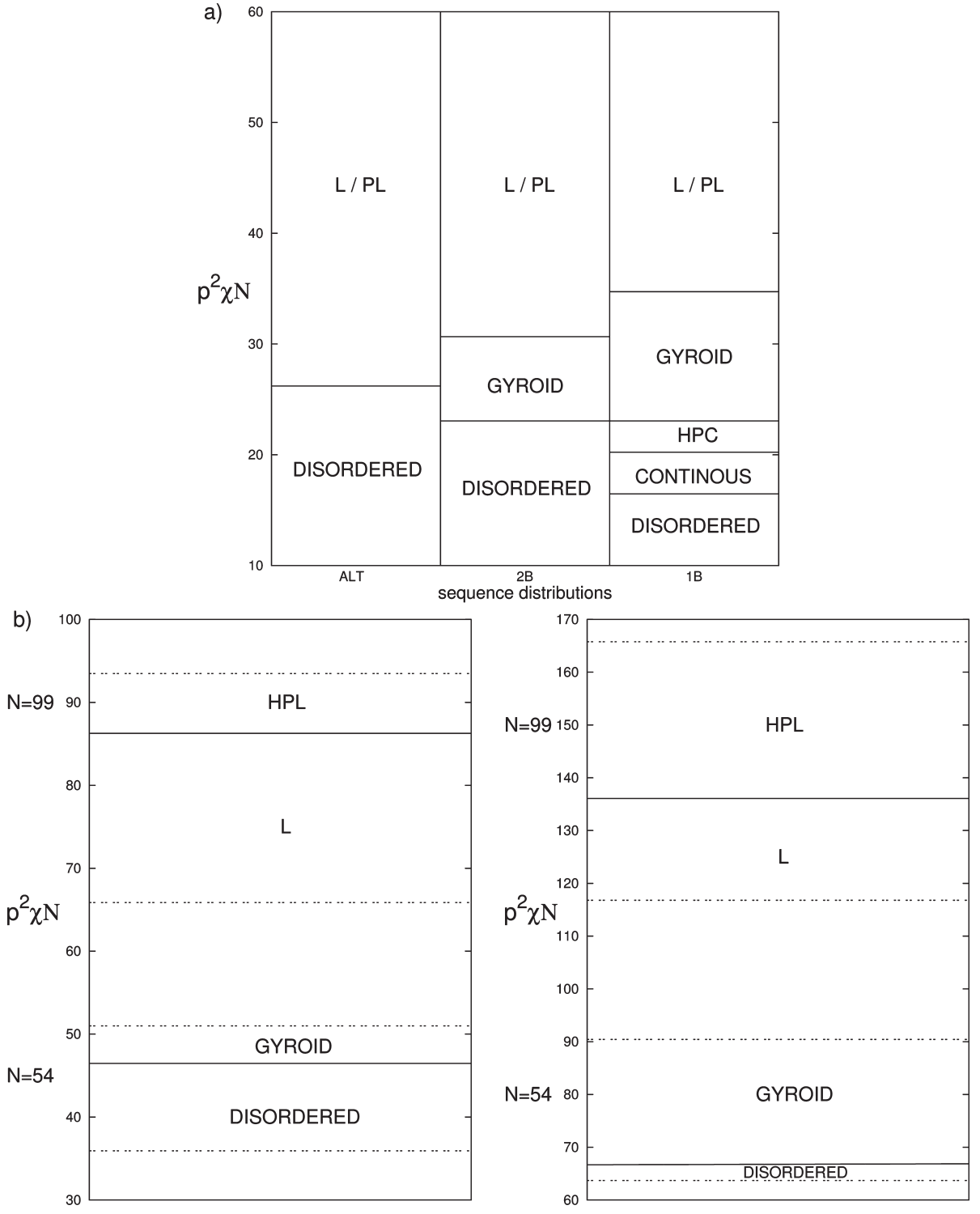

Figure 9. (a) Phase diagram for ALT, 2B, and 1B with realistic ϵ values in terms of $p^2\chi N$. (b) Experimental phase diagram in terms of $p^2\chi N$ for $p = 0.38$ (left-hand side panel) and $p = 0.51$ (right-hand side panel), showing phase transitions (solid lines) and limits of the experimental window (dashed lines).

simulations. Whereas there is clearly quantitative discrepancy between simulations and experiments, there is some encouraging qualitative agreement.

The formation of lamellar phases is seen in all of the simulations and experiments at high values of $p^2\chi N$. The formation of the gyroid phase at the ODT is seen in 2B and in the experiments. The complexity of phase behavior seen in 1B is not in agreement with experiments. The continuous phase, which we have not been able to identify clearly, forms in a narrow window neighboring the disordered phase in 1B. Perhaps poorly defined morphologies seen under these conditions are due to weak driving forces. Comparing the results in Figure 9a,b suggests that the PSS−PMB copolymers exhibit behaviors that are intermediate between ALT and 2B. We certainly do not claim that the experimental system is similar to sample 2B. The experimental system is undoubtedly highly complex, comprising a large variety of chains, which is consistent with the synthesis approach. Our work merely suggests that blocky sequence distributions may play a role in determining the phase behavior of these systems. It is important to note that our estimate of χ in ref 16 is based on the assumption of random

sulfonation. If the chains are blocky, then a more refined approach[24−27] is needed to obtain χ. It is also conceivable that different synthesis protocols lead to different degrees of blockiness, which may have led to the large variation in the measured values of χ between PS and PSS.[19,20] Our work (Figure 9) also provides a qualitative explanation for the observation of lamellar phases in the strongly segregated, symmetric partially sulfonated block copolymers studied in ref 34.

IV. Conclusions

We performed MC lattice simulations to obtain a fundamental understanding of the factors that govern the experimentally observed phase behavior of symmetric PSS−PMB copolymers.[16] We studied the effect of sequence distribution of the sulfonated PSS segments, which exhibits extremely repulsive interactions with both PS and PMB monomers (χ is of order six) by considering an alternating copolymer (ALT), a block where the sulfonated monomers are present in the form of two roughly equal length sub-blocks (2B), and one where the sulfonated monomers are present in the form of one sub-block in the middle of the sulfonated block (1B). The ALT and 2B simulations captured many of the qualitative features observed in PSS−PMB copolymers. The simulations of ALT and 2B exhibited L/PL, G, and disordered phases that were similar to those observed experimentally. 1B exhibited much richer behavior and exhibited four ordered phases: a continuous phase, hexagonally packed cylinders, G, and L/PL. The phases obtained for 2B and 1B sequence distributions can be interpreted to be those for pentablock and triblock melts, respectively. Whereas the full phase diagrams for those multiblock melts have not been worked out, the presence of both lamellar and nonlamellar phases observed at a fixed volume fraction of S of 21% is, perhaps, surprising.

We have answered the three questions posed in the Introduction. The answers are: (1) It is clearly meaningful to use χ parameters as high as six in simulations to predict the phase behavior of complex copolymers such as PSS−PMB. The large discrepancy in the values of χ reported in the literature may be due to the blocky nature of the PSS block. (2) The simulations based on χ parameters alone do explain the presence of nonlamellar phases in symmetric PSS−PMB copolymers. Whereas there is no doubt that more elaborate models with dipolar interactions will be needed for understanding the quantitative aspects of the phase behavior of PSS−PMB copolymers, the present model represents the first step toward understanding the properties of ion-containing block copolymers. (3) The simulations clearly show that sequence effects are extremely important, especially when the monomers of interest exhibit very large χ parameters. Independent experiments quantifying the blockiness of the PSS chains are clearly needed.

Acknowledgment. P.K. and M.B. gratefully acknowledge the computational grant from the Supercomputing and Networking Center (PCSS) in Poznan, Poland. M.J.P. and N.P.B. were supported by a grant from the National Science Foundation (CTS 0625785) and the Electron Microscopy of Soft Matter Program at Lawrence Berkeley National Laboratory (LBNL) supported by the Director, Office of Science, Office of Basic Energy Sciences, Materials Sciences and Engineering Division of the U.S. Department of Energy under contract no. DE-AC02-05CH11231. This work was initiated at a joint Poland−U.S. workshop on nanomaterials organized by Dr. Robert M. Wellek and sponsored by the U.S. National Science Foundation.

References and Notes

(1) Hickner, M. A.; Ghassemi, H.; Kim, Y. S.; Einsla, B. R.; McGrath, J. E. *Chem. Rev.* **2004**, *104*, 4587.
(2) Mauritz, K. A.; Moore, R. B. *Chem. Rev.* **2004**, *104*, 4535.
(3) Kreuer, K. D. In *Handbook of Fuel Cell: Fundamentals, Technology, and Applications*; Vielstich, W., Lamm, A., Gasteiger, H. A, Eds.; Wiley: Chichester, England, 2003; Vol. *3*.
(4) Leibler, L. *Macromolecules* **1980**, *13*, 1602.
(5) Fredrickson, G. H.; Helfand, E. *J. Chem. Phys.* **1987**, *87*, 697.
(6) Bates, F. S.; Fredrickson, G. H. *Annu. Rev. Phys. Chem.* **1990**, *41*, 525.
(7) Matsen, M. W.; Bates, F. S. *Macromolecules* **1996**, *29*, 1091.
(8) Matsen, M. W.; Bates, F. S. *J. Chem. Phys.* **1997**, *106*, 2436.
(9) Cochran, E. W.; Garcia-Cervera, C. J.; Fredrickson, G. H. *Macromolecules* **2006**, *39*, 2449.
(10) Floudas, G.; Ulrich, R.; Wiesner, U. *J. Chem. Phys.* **1999**, *110*, 652.
(11) Hillmyer, M. A.; Maurer, W. W.; Lodge, T. P.; Bates, F. S.; Almdal, K. *J. Phys. Chem. B* **1999**, *103*, 4814.
(12) Ruegg, M. L.; Reynolds, B. J.; Lin, M. Y.; Balsara, D. J. L. N. P. *Macromolecules* **2007**, *40*, 1207.
(13) Lennon, E. M.; Katsov, K.; Fredrickson, G. H. *Phys. Rev. Lett.* **2008**, *101*, 138302.
(14) Micka, U.; Binder, K. *Macromol. Theory Simul.* **1995**, *4*, 419.
(15) Vassiliev, O. N.; Matsen, M. W. *J. Chem. Phys.* **2003**, *118*, 7700.
(16) Park, M. J.; Balsara, N. P. *Macromolecules* **2008**, *41*, 3678.
(17) Robinson, R. A.; Stokes, R. H. In *Electrolyte Solutions*; Academic Press: New York, 1955.
(18) Banaszak, M.; Clarke, J. *Phys. Rev. E* **1999**, *60*, 5753.
(19) Tan, N. C. B.; Briber, X. L. R. M.; Peiffer, D. G. *Polymer* **1995**, *36*, 525.
(20) Zhou, N. C.; Xu, C.; Burghardt, W. R.; Composto, R. J.; Winey, K. I. *Macromolecules* **2006**, *39*, 2373.
(21) Pakula, T. *Macromolecules* **1987**, *20*, 679.
(22) Pakula, T. Chapter 5. In *Simulation Methods for Polymers*; Kotelyanskii, M. J., Thedorou, D. N., Eds.; Marcel-Dekker: New York, 2004.
(23) Banaszak, M.; Wołoszczuk, S.; Pakula, T.; Jurga, S. *Phys. Rev. E* **2002**, *66*, 031804.
(24) Shakhnovich, E. I.; Gutin, A. M. *J. Physiol.* (*Paris*) **1989**, *50*, 1843.
(25) Fredrickson, G. H; Milner, S. T.; Leibler, L. *Macromolecules* **1992**, *25*, 6341.
(26) Qi, S.; Chakraborty, A. K.; Wang, H.; Lefebvre, A. A.; Balsara, N. P.; Shakhnovich, E. I.; Xenidou, M. M.; Hadjichristidis, N. *Phys. Rev. Lett.* **1999**, *82*, 2896.
(27) Eitouni, H. B.; Rappl, T. J.; Gomez, E. D.; Balsara, N. P.; Qi, S.; Frechet, A. K. C. J. M. J.; Pople, J. A. *Macromolecules* **2004**, *37*, 8487.
(28) Larson, R. G. *J. Chem. Phys.* **1992**, *96*, 7904.
(29) Tries, V.; Paul, W.; Baschnagel, J.; Binder, K. *J. Chem. Phys.* **1997**, *106*, 738.
(30) de Gennes, P.-G. *Scaling Concepts in Polymer Physics*; Cornell University Press: Ithaca, NY, 1979.
(31) Banaszak, M.; Wołoszczuk, S.; Jurga, S.; Pakula, T. *J. Chem. Phys.* **2003**, *119*, 11451.
(32) Woloszczuk, S.; Banaszak, M.; Knychala, P.; Radosz, M. *Macromolecules* **2008**, *41*, 5945.
(33) Eitouni, H. B.; Balsara, N. P. Chapter 19. In *Physical Properties of Polymer Handbook*; Mark, J. E., Ed.; Springer: New York, 2007.
(34) Rubatat, L.; Li, C.; Dietsch, H.; Nykanen, A.; Ruokolainen, J; Mezzenga, R. *Macromolecules* **2008**, *41*, 8130.